

The formation of massive stars: accretion, disks, and the development of hypercompact H II regions

Eric Keto

Harvard-Smithsonian Center for Astrophysics, 60 Garden St., Cambridge, MA 02138

ABSTRACT

The hypothesis that massive stars form by accretion can be investigated by simple analytical calculations that describe the effect that the formation of a massive star has on its own accretion flow. This paper investigates the effects of the ionizing radiation of a massive star forming within a very simple accretion model that includes angular momentum, that of gas flow on ballistic trajectories around a star. Very different H II region morphologies, that might appear to indicate different underlying models, may be related to this same basic accretion flow model with different model parameters. The hypercompact H II regions may be related to, and perhaps theoretically defined as, those H II regions associated with massive stars that are still growing by accretion.

Subject headings: stars: early type | stars: formation | ISM : H II regions

1. Introduction

The hypothesis that massive stars form by accretion can be investigated by simple analytical calculations that describe the effect that the formation of a massive star has on its own accretion flow. An earlier paper (Keto 2002b) studied the effect of star formation in a spherically-symmetric, steady-state flow (Bondi 1952) and showed how, under certain conditions, a molecular accretion flow may pass through an ionization front and continue toward the star as an ionized accretion flow. In this case, the H II region is the ionized inner zone of a continuous accretion flow. More generally, angular momentum in an accretion flow will result in a flattened geometry with different consequences for the structure of the ionized accretion flow and H II region.

This paper investigates the effects of the ionizing radiation of a massive star forming within a very simple accretion model that includes angular momentum, that of gas flow on

ballistic trajectories around a star (Ulrich 1976). The investigation suggests how H II regions with a variety of structures can be produced by the variation of the several parameters describing the flow and the star: the gas density in the flow, the angular momentum, the mass of the star, and the flux of ionizing radiation. Very different H II region morphologies, that might appear to indicate different underlying models, can be produced by the same basic accretion flow model with different model parameters. In particular, by increasing the ionizing flux of a model star and thus the radius of ionization, as would happen as a star that is growing by accretion gains mass, a model H II region may be evolved from a gravitationally trapped H II region as described in Keto (2002b, 2003), through a bipolar morphology, and finally into a photo-evaporating disk as described by Hollenbach et al. (1994), Yorke (1995), Yorke & Welz (1996), Lizano et al. (1996), Johnstone, Hollenbach, & Bally (1998), and Lugo, Lizano & Garay (2004).

The different forms of H II regions produced by the variation of the model parameters may be compared with observed H II region morphologies. Because the size scales are rather small, less than a few thousand AU, on which the gravitational force of one or more massive stars affects the dynamics of the hot ionized gas, these H II regions within accretion flows must relate to the smallest H II regions (size scales < 0.01 pc), the observationally defined hypercompact H II regions (Kurtz 2000). Thus the hypercompact H II regions may be related to, and perhaps theoretically defined as, those H II regions associated with massive stars that are still growing by accretion.

2. Relevant results from the spherical model: the 3 evolutionary stages of an H II region

Stellar structure models suggest that massive stars that form by contraction have a very short pre-main sequence phase (PMS), and that those that form by accretion have no PMS phase at all because the star begins hydrogen burning while still accreting (Palla & Stahler 1993; Beech & Mitani 1994; Behrend & Mader 2001; Bermanconi & Mader 1996; Norberg & Mader 2000). These calculations suggest that a massive star that is forming by accretion will reach the main sequence with a mass below that which would produce sufficient ionizing radiation to maintain an H II region around the star. The non-existent H II region at this stage may be described as quenched (Walmsley 1995). Because the production of ionizing photons increases as a higher power of the stellar mass than does the accretion rate, eventually the flux of ionizing radiation, J , from a star that is gaining mass by accretion, will exceed the flux of neutral gas onto the star (Keto 2003),

$$J > 4 r^2 n_H v \tag{1}$$

where r is the stellar radius, n_H is the the number density of neutral gas, and v the inflow velocity.

If the density of the accretion flow decreases no faster than $r^{-3/2}$, then the H II region that develops in the flow will be bounded at a distance, R_i (Franco, Tenorio-Tagle & Bodenheimer 1990), defined by the balance of the ionizations and recombinations (Spitzer 1978, eqn. 5.20),

$$\int_r^{R_i} 4 r^2 n_e^2(r) \, dr = 0 \quad (2)$$

This equation incorporates the "on-the-spot" approximation with the recombination rate to all Rydberg levels of H above the first level, $n = 1$.

The small H II region that develops just as the quenched phase (equation 1) ends cannot expand hydrodynamically because the outward pressure of the ionized gas is less than the inward gravitational force of the star. Instead, the neutral accretion flow passes through the ionization front and continues on to the star as an ionized accretion flow. The H II region at this stage may be described as gravitationally trapped (Keto 2002b). As the star continues to gain mass and its flux of ionizing radiation increases, the boundary of the H II region, set by ionization equilibrium rather than pressure balance, will be found at greater radii. Once a radius is reached where the escape velocity from the star is below the sound speed of the ionized gas, the H II region will begin to expand hydrodynamically. This radius is approximately equal to the Bondi-Parker critical radius where the velocity of the incoming accretion flow first reaches the sound speed of the ionized gas,

$$R_b = GM = 2c^2 \quad (3)$$

where M is the mass of the star and c is the sound speed. The evolution of the H II region then transitions to a phase of pressure-driven expansion in which the gravitational attraction of the star is negligible over most of the H II region. These pressure dominated H II regions are adequately described by models with no gravitational force (Spitzer 1978; Dyson & Williams 1980; Shu 1992). The model for the development of an H II region within a spherical accretion flow thus suggests three stages: 1) quenched or non-existent, 2) gravitationally trapped, and 3) pressure driven-expansion. The divisions between the stages occur when the radius of ionization equilibrium, R_i , (equation 2) which increases as the star gains mass by accretion, exceeds first the stellar radius, R_* , and second the Bondi-Parker critical radius, R_b (equation 3).

3. A non-spherical accretion flow

One simple model of accretion that includes rotation equates the stream lines of an accretion flow with ballistic trajectories around a point mass Ψ (Ulrich 1976; Cassen & Moosman 1981; Terebey, Shu & Cassen 1984). The flow is determined by the gravitational attraction of the point source subject to conservation of angular momentum and mass. In particular, the model ignores the pressure and self-gravity of the gas. The initial distribution of angular momentum is that of solid body rotation on an arbitrary radius or conceptual spherical surface some distance from the star. Thus on each trajectory, the specific angular momentum, $v r \sin \theta_0$, where θ_0 is the initial polar angle. An accretion disk develops from the flattening of the flow as determined by the initial angular momentum and from the assumption that where the trajectories would cross the equatorial plane, the flow is met by a symmetrically opposing flow. The equations for the velocity and density at a position $(r; \theta)$ are Ψ (Ulrich 1976),

$$v_r = \frac{GM}{r} \frac{1-\cos^2 \theta}{1 + \frac{\cos^2 \theta}{\cos^2 \theta_0}} \quad (4)$$

$$v_\theta = \frac{GM}{r} \frac{\sin^2 \theta}{(\cos \theta_0 \cos \theta)} \frac{1 + \frac{\cos \theta_0 + \cos \theta}{\cos \theta_0 \sin \theta}}{1-\cos^2 \theta} \quad (5)$$

$$v_\phi = \frac{GM}{r} \frac{\sin^2 \theta_0}{\sin \theta} \frac{1 + \frac{\cos \theta}{\cos \theta_0}}{1-\cos^2 \theta} \quad (6)$$

where,

$$r = \frac{R_d \cos \theta_0 \sin^2 \theta}{\cos \theta} \quad (7)$$

This last equation includes the parameter, R_d , which is the radius at which the gravitational force equals to the centrifugal force in the mid-plane,

$$\frac{GM}{R_d^2} = \omega^2 R_d \quad (8)$$

This radius, approximately where the accretion flow transitions from a quasi-spherical inflow to a rotationally supported disk, may also be written analogously with the Bondi-Parker transonic radius as,

$$R_d = \frac{GM}{v^2} \quad (9)$$

where v , the orbital velocity at R_d , replaces the sound speed in equation 3. The gas density is found from mass conservation (Mendoza, Canto, Raga 2004),

$$n = n_0 r_0^{-3} \frac{1 + \frac{\cos^2 \theta}{\cos^2 \theta_0}}{1 + \frac{r_0}{r} (3 \cos^2 \theta_0 - 1)} \quad (10)$$

4. The development of an H II region in the non-spherical accretion flow

An H II region will develop at the center of the flow defined by equations 4 through 10 once the ionizing flux of the accreting star satisfies the condition in equation 1. However, in a non-spherical flow, the gas density is not radially symmetric, and therefore the H II boundary, R_i , is at larger distances in directions where the gas density is lower. In the axially symmetric model above, the boundary is therefore a function of the polar angle, θ . The spherical model of x2 suggests that if $R_i > R_b$ the H II region expands hydrodynamically. In the non-spherical model, this condition is a function of the polar angle, θ . Thus while somewhat idealized, in the non-spherical model the H II region may be expanding over a range of θ about the polar axis while the accretion flow continues to flow into and through the H II in a range of θ around the plane of the disk.

This simple model of the ionization of an accretion flow does not explicitly include the effect of a stellar wind on the H II region. However, we know that naked (unembedded) early-type stars produce powerful winds that at their terminal velocities have mechanical energies, v_t^2 (Lamers & Cassinelli 1999), that exceed the mechanical energies of star-forming accretion flows. However, because the winds accelerate on the surface of the star the wind energy is negligible near the star and, in the idealized spherical model, the wind may be suppressed by the accretion flow. Once inflow ends because the gas within the H II region begins expanding ($R_i > R_b$), the wind may be expected to break out and dominate the hydrodynamics. Thus in the non-spherical model, the following approximation is adopted. At a polar angle, θ , where $R_i(\theta) > R_b$, the inflow is replaced by the simplest model of a stellar wind (Parker 1958). This wind solution is the analogue of the Bondi accretion flow and described by the same equation,

$$\frac{d}{dr} \frac{v^2}{2} + \frac{dP}{dr} + \frac{GM}{r^2} = 0 \tag{11}$$

but with the boundary conditions that the flow is subsonic at the stellar surface and supersonic beyond the transonic radius. In the case of non-spherical flows, the location of the transonic radius depends on the geometry of the flow, specially on the divergence of the stream lines about the star (Kopp & Holzer 1976). However, if the divergence is approximately spherical, the transonic point will be approximately located by equation 3. For simplicity, this approximation is adopted. The resulting model of a wind in the polar directions and accretion at lower latitudes is inconsistent in that the wind solution is driven by hydrodynamic pressure, but in the accretion flow, the pressure is neglected. Nonetheless, the examples in x6 will show that this approximation is useful on a conceptual level and produces models that describe the morphology of observed H II regions.

5. The 3 R 's of hypercompact H II regions

The equations in sections 2 and 4 fully describe the model of an H II region in a non-spherical accretion flow. The morphology of the H II region depends on several physical quantities that are specified as parameters of the model, the mass of the star, the gas density and angular momentum in the accretion flow, and the flux of ionizing radiation from the star. Because these physical quantities have different units, it is helpful to organize them into parameters of the same physical dimension as 3 characteristic radii. The radius of disk formation, R_d (equation 9), along with the Bondi-Parker radius, R_b (equation 3), and the radius of ionization equilibrium, R_i (equation 2), may be called the 3 R 's of H II regions in that they describe the basic structure of the accretion flow.

6. Examples and evolution

6.1. Ionization

The first example illustrates the effect of increasing the ionizing flux within the same accretion flow. Figure 1 (left) illustrates a model flow and H II region with a stellar mass of $18 M_\odot$ and a flux of ionizing radiation of 10^{45} photons s^{-1} corresponding to a B0.5 star, a specific angular momentum of $\dot{p}_0 = 0.04 \text{ km s}^{-1} \text{ pc}$, $R_d = 42 \text{ AU}$, $R_b = 43 \text{ AU}$, and a gas density, n_0 of 10^7 cm^{-3} . The density n_0 in the flow (equation 10) is approximately the density at R_b , or precisely $n = n_0 \sqrt{2} = 3$ at R_b (Mendoza, Canto, Raga 2004) on the polar axis (prior to substitution of the wind solution).

At this flux level and density, although the H II region has a slightly bipolar shape owing to the flattening of the flow, $R_i < R_b$ at all polar angles. Thus the H II region is trapped within the gravitational field of the star, and accretion may proceed through the H II region at all angles. Increasing the stellar mass to $22 M_\odot$ and the flux of ionizing radiation to 10^{47} photons s^{-1} , corresponding to an O9 star, results in a model with $R_i > R_b$ everywhere except at a narrow range of angle just around the disk (figure 1 right). Thus an increase in the flux of ionizing radiation corresponding to an increase in mass changes the H II region from gravitationally trapped within the accretion flow to expanding around a thin molecular accretion. This latter structure is essentially the same structure as assumed in the photo-evaporating disk model (Hollenbach et al. 1994; Yorke 1995; Yorke & Welz 1996; Lizano et al. 1996; Johnstone, Hollenbach, & Bally 1998; Lugo, Lizano & Garay 2004). Thus a gravitationally trapped H II region and a photo-evaporating disk may be different expressions of the same model of an H II region within an accretion flow. Furthermore, the two may be related as earlier and later evolutionary stages of the development of the H II region within the flow.

In this idealized model, as the ionizing radiation from the star increases, the H II region begins its evolution bounded with a shape that evolves from nearly spherical to increasingly bipolar. Once the tip of the bipolar lobes reaches the Bond-Parker critical radius, the H II transitions to an unbounded morphology with a narrow opening angle defined by the condition, $R_i(\theta) > R_b$. As the ionizing flux increases further, the opening angle also increases until finally all that remains of the molecular accretion flow is confined to the disk in the mid-plane. In this scenario, the bipolar phase is relatively brief in the evolution between the gravitationally trapped and photo-evaporating disk phases. In the specific model above, the bipolar phase corresponds to a range of stellar mass between 20 and 22 M_\odot .

6.2. Angular momentum

The second example shows the effect of different values of the angular momentum on the structure of the accretion flow. Flows that have relatively low angular momentum will produce what may be described as a fat accretion torus around the growing star while those with relatively high angular momentum will produce a thin disk. Because the density of the flow increases inward following mass conservation regardless of the angular momentum, the difference between the two cases relates to where in the flow the gas density becomes observationally significant with respect to the attenuating of the flow. The flow becomes observable as the gas density approaches the critical density for collisional de-excitation, $n_c = A_{ij}/C_{ij}$, where A_{ij} is the Einstein A coefficient and C_{ij} is the collision rate ($\text{cm}^3 \text{sec}^{-1}$) for the particular molecular tracer employed in an observation. In a model with low angular momentum, the gas will reach the critical density before attenuating into a disk, and the molecular accretion disk will be detected as a quasi-spherical rotating flow or fat torus. In the high angular momentum case, the flow will form a disk before the gas density in the surrounding flow exceeds the critical density. In this case the observations will tend to see the attenuated disk.

Figure 2 shows two variations of the same model. Both models include a star of 20 M_\odot and flux of ionizing radiation of $3 \times 10^6 \text{ photons s}^{-1}$ corresponding to type B0 (0.95). At this mass, $R_b = 54 \text{ AU}$. The model illustrated in the left column has a relatively low angular momentum, $\dot{M}_0 = 0.04 \text{ km s}^{-1} \text{ pc}$, while the model shown in the right column has a rotation rate that is 4 times higher. The values of R_d are therefore 38 AU and 609 AU respectively. The low angular momentum accretion flow is similar to the flow in the previous example. Because of the greater inward increase in the gas density in the attenuated high angular momentum flow, the density in this flow is set lower, $n = 3 \times 10^6 \text{ cm}^{-3}$, rather than $n_0 = 3 \times 10^7 \text{ cm}^{-3}$, so that similar densities are maintained at the center of the flow, and

therefore, similar opening angles for the bipolar outflow.

The 3 figures for each of the two flows show: 1) the log of the density of the molecular gas in a slice in the XZ plane, 2) simulated spectra of $\text{NH}_3(1,1)$, and 3) the first moment of the line of sight velocity field along with contours of the column density of ionized gas. The $\text{NH}_3(1,1)$ spectra are calculated using the methods described in Keto et al. (2004) with the LTE approximation as in Keto (1990). The figures of the density and the spectra suggest that observations of the high angular momentum flow would show a more attenuated structure. The spectra and first moment figures show that observations would nonetheless suggest a rotating accretion flow in both cases. Thus accretion disks and "fat toroids" may simply be different expressions of the same model accretion flow with different values of the angular momentum or equivalently different values of R_d with respect to R_b .

The spectra of $\text{NH}_3(1,1)$ is complex with 5 hyperfine lines (Ho & Townes 1983) and requires some explanation. The 2 bright lines seen in figure 2 (middle) near the central velocity are the same main hyperfine that shows up at 2 velocities red and blue-shifted by the infall and rotation of the accretion flow. The asymmetry of the lines, best seen off the center, indicates rotation. The increasing width of the lines toward the center indicates infall.

In the first-moment velocity figures there is some difference in the velocity fields. In both low and high angular momentum cases, the most red-shifted velocities occur where the infall and rotation add together along the line of sight. In the low angular momentum case, the infall, highest toward the center of the flow, combines with the rotation to place the most red-shifted velocity closer to the flow center. Even so, the observation is dominated by the red-blue shift across the map, indicative of rotation. In the high angular momentum flow, the infall is less significant and the velocity pattern is dominated by rotation.

7. Hypercompact as gravitationally dominated H II regions

The morphologies produced by models of H II regions developing within accretion flows are potentially quite varied and match many of the observed morphologies, particularly those observed at the smallest scales. In particular, the bipolar H II regions are predominantly a small scale phenomenon. For example, there is no classification for bipolar morphology in the Wood & Churchwell (1989) and Kurtz et al. (1994) survey of ultracompact H II regions whereas Depree et al. (2005) found it necessary to introduce this class to describe the morphologies of hypercompact H II regions.

The size scale of < 0.01 pc (2000 AU) suggested as the upper limit of the hypercompact

size (Kurtz 2000) is about 20 times the radius, R_b , around a single massive star. What then is the relevance of the stellar gravitational attraction on most observed H II regions?

First, O stars do not appear to form alone, but in small groups or clusters of early type stars that may also contain some number of lower mass stars. The radius, R_b , scales with the attracting mass. Groups or small clusters of stars with up to 500 – 1000 M_\odot contained within a common H II region are suggested by observations of a few of the brightest H II regions that show molecular or ionized accretion on scales of 10^3 AU (Zhang & Ho 1997; Young, Keto & Ho 1998; Keto 2002a; Sollins et al. 2005; Keto & Wood 2006). Thus the stellar gravitational attraction of groups or small clusters may be significant even on the size scales of ultracompact H II regions.

Second, the H II region need not be strictly smaller than R_b for the stellar gravitational attraction to affect its structure. For example, if the H II region is in effect an expanding wind, as in the model shown in figure 1 (right), then because the wind solution is approximately hydrostatic inside of R_b , the center of the H II region will be quite dense even though the boundary, $R_i > R_b$. For other model outflows, a steep density gradient with R_b as a characteristic radius is similarly inevitable. Then, depending on the size and density of the H II region beyond R_b , this small, high density region may be the most significant emission in an observation, particularly in radio interferometric observations. High frequency observations might then show a spatially unresolved bright core with the apparent size scale of the observing beam. Low frequency observations would show the surrounding low-level extended emission because the relative brightness of the core is much reduced by the higher optical depth at low frequency.

Certainly, the hypercompact H II regions become much more interesting and significant if their dynamics are different than the pressure dominated compact and larger H II regions. Thus the possible definition of a hypercompact H II region as one in which gravitational forces are significant is more interesting than the strictly phenomenological definition based on an even power of 10 in pc, namely (10^{-2}).

REFERENCES

- Beech, M., & Mitalas, R., 1994, *ApJ Suppl.*, 95, 517
 Behrend, A. & Maeder, A., 2001, *AA*, 373, 190
 Bemasconi, P. & Maeder, A., 1996, *AA*, 307, 839

- Beltr'an, M .T ., Cesaroni, R ., Neri, R ., Codella, C ., Funuya, R .S ., Testi, L . & O ln i, L . 2004, *ApJ*, 601, L187
- Bondi, H ., 1952, *M N R A S*, 112, 195
- Cassen, P . & M oosm an, A ., 1981, *Icarus*, 48, 353
- DeP ree, C G ., W ilner, D J ., Deblasio, J ., M ercer, A J ., D avis, L E ., 2005, *ApJL*, 624, L101
- Dyson, J. & W illiam s, D A ., 1997, *The Physics of the Interstellar M edium*, H alsted: N Y
- H ofner, P ., Cesaroni, R ., Rodriguez, L F ., M arti, J ., 1999, 345, L43
- Franco, J., Tenorio-Tagle, G . & Bodenheimer, P ., 1990, *ApJ*, 349, 126
- H o, P .T .P . & Townes, C H ., 1983, *ARAA*, 21, 239
- Hollenbach, D ., Johnstone, D ., Lizano, S ., Shu, F ., 1994, *ApJ*, 428, 654
- Johnstone, D ., Hollenbach, D ., & Bally, J ., 1998, *ApJ*, 499, 758
- Keto, E ., 1990, *ApJ*, 355, 190
- Keto, E ., 2002a, *ApJ*, 568, 754
- Keto, E ., 2002b, *ApJ*, 580, 980
- Keto, E ., 2003, *ApJ*, 599, 1196
- Keto, E ., Rybicki, G ., Bergin, E A ., Plum e, R ., 2004, *ApJ*, 613,355
- Keto, E . & W ood, K ., 2006, *ApJ*, 637, 850
- Kopp, R A . & Holzer, T E ., 1976, *Solar Physics*, 49, 43
- Kurtz, S., Churchwell, E ., W ood, D O S ., 1994, *ApJS*, 91, 659
- Kurtz, S., 2000, *RevM exA A*, 9, 169
- Lam ers, H . & Cassinelli, J ., 1999, *Introduction to Stellar W inds*, C am bridge U niv. P ress
- Lizano, S ., Canto, J ., G aray, G ., Hollenbach, D ., 1996, *ApJ*, 465, 216
- Lugo, J., Lizano, S ., G aray, G ., 2004, *ApJ*, 614, 807
- Norberg, P . & M aeder, A ., 2000, *AA*, 359, 1025

- Mendoza, S., Canto, J., Raga, A.C., 2004 *Rev. Mex. AA*, 40, 147
- Palla, F., & Stahler, S., 1993, *ApJ*, 418, 414
- Sollins, P., Zhang, Q., Keto, E., Ho, P., 2005, *ApJ*, 624, L49
- Shu, F., 1992, *The Physics of Astrophysics, Volume II, Gas Dynamics*, University Science Books, Mill Valley, CA
- Spitzer, L., Jr., 1978, *Physical Processes in the Interstellar Medium*, (New York: Wiley)
- Terebey, S., Shu, F., Cassen, P., 1984 *ApJ*, 286, 529
- Ulrich, R., 1976, *ApJ*, 210, 377
- Vacca, W.D., Garmany, C.D. & Shull, J.M., 1996, *ApJ*, 460, 914
- Walmley, M., 1995, *Revista Mexicana de Astronomía y Astrofísica Serie de Conferencias*, Vol. 1, *Circumstellar Disks, Outflows and Star Formation*, Cozumel, Mexico, Nov 28-Dec 2, 1994, p. 137
- Wood, D.O.S., Wood & Churchwell, E., 1989, *ApJS*, 69, 831
- Young, L.M., Keto, E., Ho, P.T.P., 1998, *ApJ*, 507, 270
- Yorke, H. & Welz, A., 1996, *A & A*, 315, 555
- Yorke, H., 1995, *Rev. Mex. AA*, 1, 35
- Zhang, Q. & Ho P., 1997, *ApJ*, 488, 241

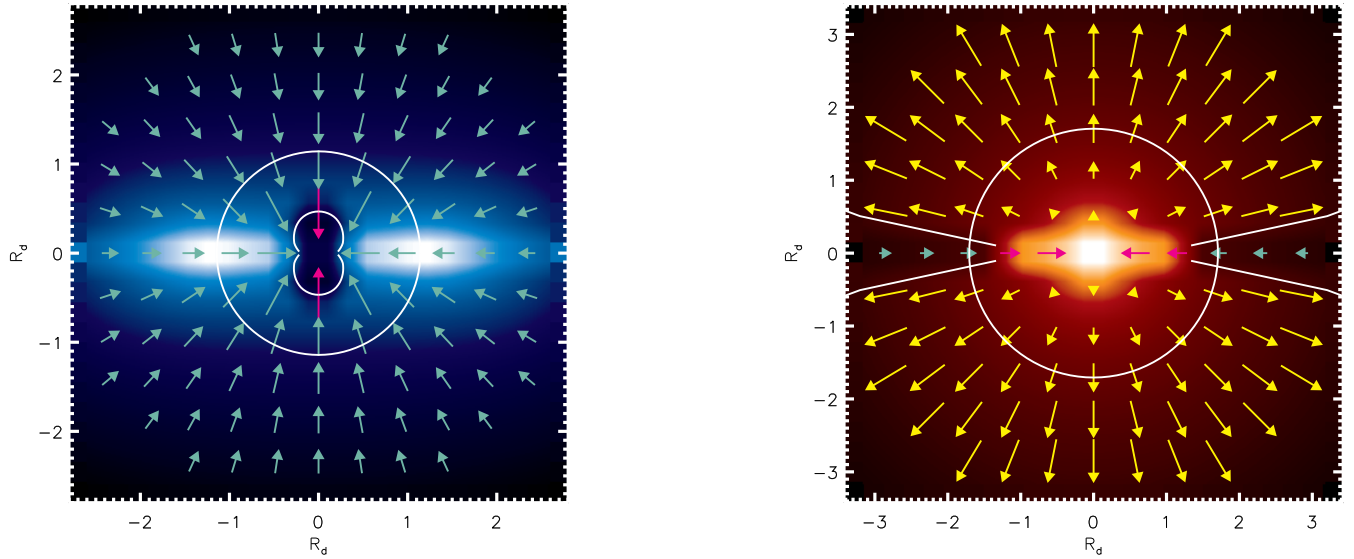


Fig. 1. | Model of a high angular momentum accretion flow subject to 2 levels of ionizing radiation, low (left) and high (right) as defined in §6. The figures show the log of the density of molecular gas in blue (left) and of the ionized gas in red (right) in a slice in the XZ plane of the flow. The color scales range from 0 to $1.6 \times 10^7 \text{ cm}^{-3}$ (left) and 0 to $1.3 \times 10^7 \text{ cm}^{-3}$ (right). The circle shows the location of the Bondi-Parker critical radius of the ionized gas for spherical flow. The arrows show the velocity of the flow in the XZ plane. The longest arrow in the molecular flow (left) represents 26.6 km s^{-1} and the longest arrow in the ionized flow represents 21.5 km s^{-1} . In the ionized flow (right) the velocity is the sound speed at the critical radius. The axes are labeled in units of R_d , 42 AU (left) and 34 AU (right).

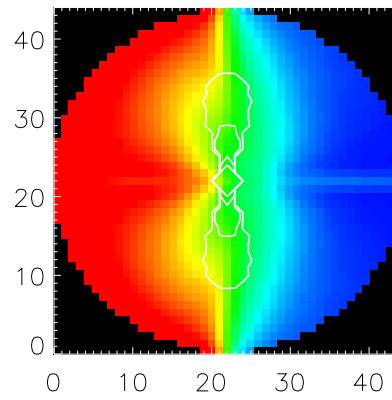
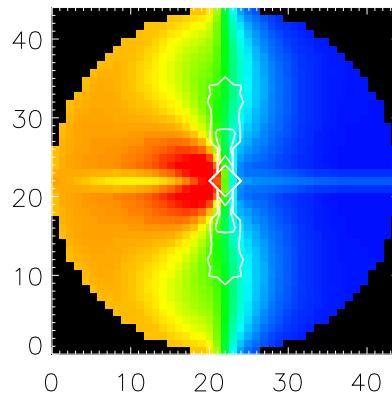
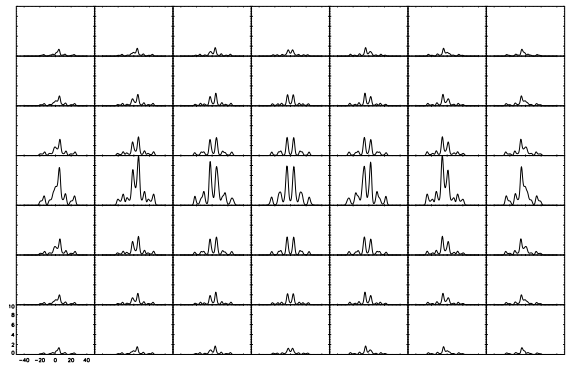
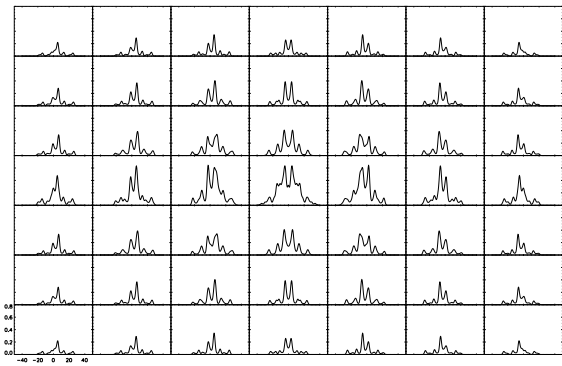
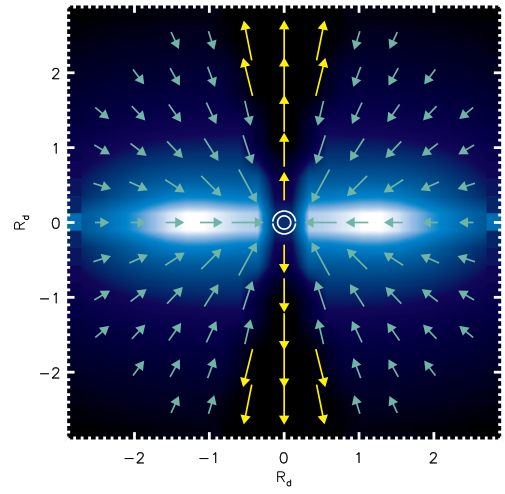
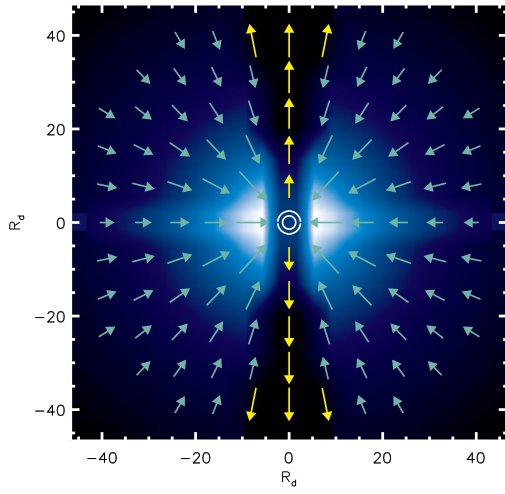


Fig. 2. | Three views of two accretion flows that differ in the relative amount of angular momentum. The flow in the right column has 4 times the angular momentum of the flow in the left column. The two top figures show a slice in the XZ plane with the log of the density of the molecular gas in color and the velocity as arrows. The density ranges from 0 to $3.6 \times 10^6 \text{ cm}^{-3}$ (left) and from 0 to $7.6 \times 10^6 \text{ cm}^{-3}$ (right). The longest arrow in the molecular flow (blue arrows) represents 6.5 km s^{-1} (left) and 10.5 km s^{-1} (right). The yellow arrows show the velocity of the ionized outflow at half the scale. The middle two panels show simulated $\text{NH}_3(1,1)$ spectra for the two flows. The horizontal axis covers 100 km s^{-1} in each panel, and the vertical axis covers 0 to 0.8 K (left) and 0 to 10.0 K (right). The spacing between the panels is 110 AU in both figures or $3 R_d$ (left) and $0.2 R_d$ (right). The bottom panels show the first moment of the line-of-sight velocity in color and the contours of the column density of the ionized gas. The color scale ranges from -4.7 to 4.5 km s^{-1} (left) and -4.1 to 3.9 km s^{-1} (right). The contours are logarithmic at $-6, -5, -4$ and -3 of the peak column density. A single observation would not be expected to cover such a dynamic range. A high frequency observation would see only the bright compact center. At low frequencies, because the center of the H II region would be optically thick, the relative brightness between the center and wings is reduced, and the low-level, extended emission of the outflow would be detectable.